Fabrication and characterization of microscale sandwich beams

Francisco Arias, Paul J.A. Kenis, Bing Xu, Tao Deng, Olivier J.A. Schueller, and George M. Whitesides[a)]
Department of Chemistry and Chemical Biology, Harvard University, 12 Oxford Street, Cambridge, Massachusetts 02138

Yuki Sugimura and Anthony G. Evans[b)]
Division of Engineering and Applied Sciences, Harvard University, 29 Oxford Street, Cambridge, Massachusetts 02138

(Received 10 July 2000; accepted 20 November 2000)

Microscale sandwich beams with cell diameters and wall widths down to 150 and 15 μm, respectively, and having both metallic and polymer/metal cores were produced through fabrication methods that combined photolithography and electrodeposition. Various core structures were used, including some with negative Poisson's ratio. The bending response was investigated and compared with beam-theory predictions. Most of the cores evaluated had sufficient shear stiffness that the bending compliance was relatively high and dominated by the face sheets. Two of the core configurations were "soft" and exhibited behavior governed by core shear. The relative dimensions of the cores evaluated in this study were far from those that minimize the weight, because of fabrication constraints. The development of an ability to make high-aspect ratio cores is an essential next step toward producing structurally efficient, lightweight microscale beams and panels.

I. INTRODUCTION

Sandwich construction is commonly used in structures where strength, stiffness, and weight efficiency are required.[1] Low-density, hexagonal honeycombs are preferred as the core material on a performance basis.[2] Problems with robustness and affordability, however, have prompted investigations of alternative sandwich constructions based on lightweight metallic foams and trusses.[3,4] New microfabrication techniques such as laser stereolithography,[5] UV laser ablation,[6] and lithography galvanoformung abformung (LIGA)[7] provide an opportunity to create microscale analogues of macroscopic structures with useful mechanical properties. In this article we explore a rapid prototyping strategy consisting of photolithographic, electrodeposition, and face-sheet bonding steps to fabricate microbeams consisting of a range of metallic and polymer/metallic composite core configurations sandwiched between two sheets of nickel. We also investigate the structural response—load, flexural rigidity, and failure load—of the sandwich beams in detail. For the cores we used regular hexagonal honeycombs, structures with negative Poisson ratio (NPR), structures based on various tilings, and Flexcore (Fig. 1).

The objectives of the present study are (i) to explore convenient fabrication procedures for microstructures such as sandwich beams, (ii) to measure the bending performance of fabricated microbeams, and (iii) to compare the measured load capacity and stiffness with beam theory predictions. The configurations chosen have not yet been optimized for minimum weight, wherein several failure modes would operate simultaneously.[1,2,14,15] Instead, most of the cores are overdesigned in such a way that their response should be face sheet dominated (Appendix). In a few instances, compliant cores are used, causing the bending response to be core dominated. The measurements performed on such beams probe the shear properties of these configurations.

For the exploration of these behaviors, microscale sandwich beams have been fabricated by the combination of photolithography (or soft lithography[8]), through-mask electroplating, and face-sheet bonding or soldering, very similar to the fabrication of NPR grids[9] and honeycomb sandwich panels[10] that we have reported previously. The sandwich panels in our previous studies comprised unit cells approximately 500 μm in diameter and 100 μm in wall width—typical dimensions of struc-

a)Address all correspondence to this author
b)Present address: Princeton Materials Institute, Princeton University, 70 Prospect Avenue, Princeton, New Jersey 08540

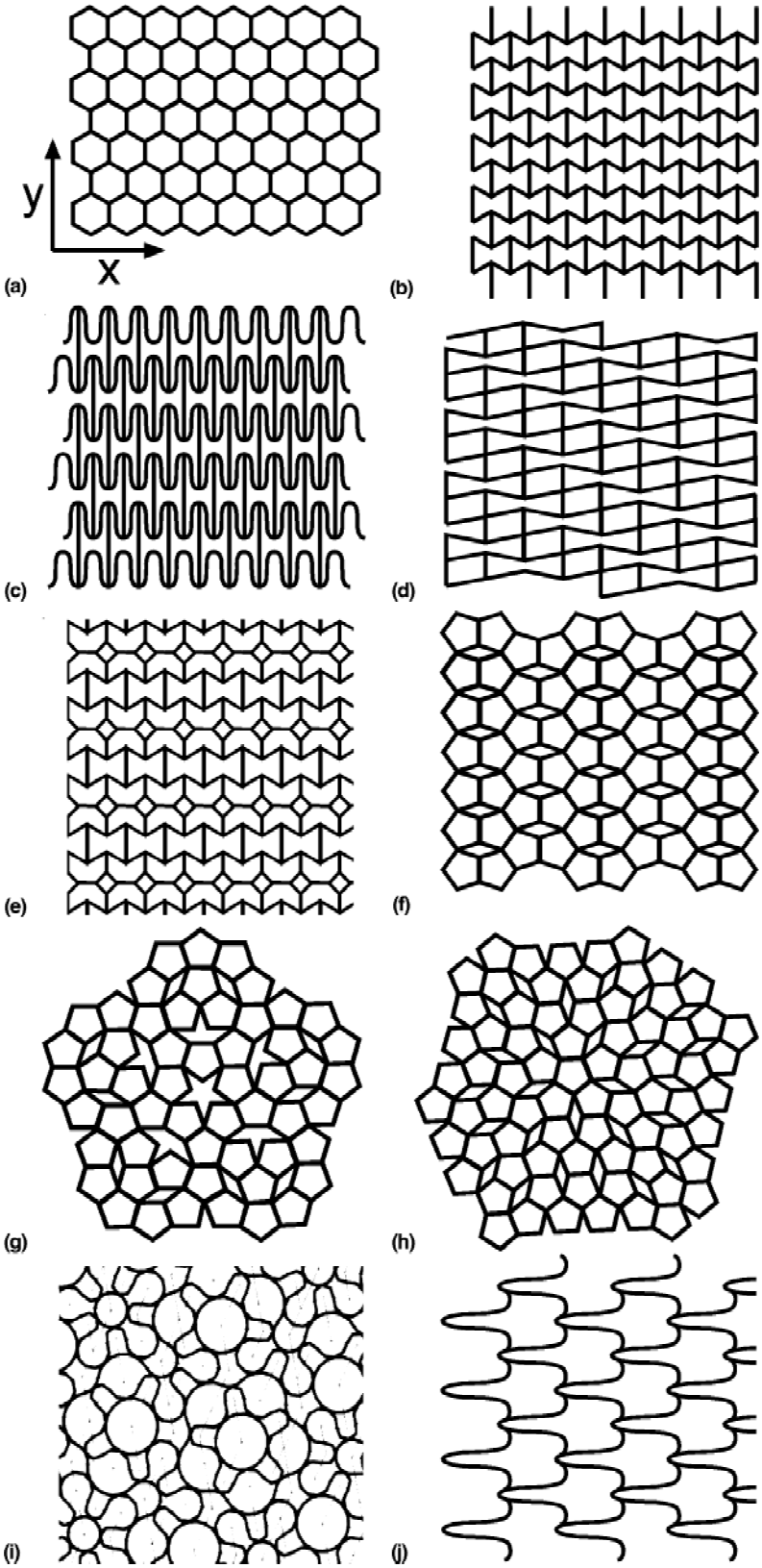

FIG. 1. Geometries used for the core of the microscale sandwich beams. The *x*- and the *y*-axes indicate the grid orientation relative to the specimen (see Fig. 4). Key: (a) regular hexagonal cells; (b) reentrant honeycomb grid with negative Poisson's ratio (NPR); (c) NPR grid where the unit cell has curved vertical sides; (d) structure that combines the square motifs and reentrant honeycombs; (e) structure that combines rhomboidal motifs and reentrant honeycombs; (f) periodic Durer's pentiling; (g) quasiperiodic Kepler's pentiling; (h) quasiperiodic Durer's pentiling; (i) penrose structure; and (j) flexcore grid.

tures made by the use of high-resolution transparency film as the mask in photolithography—with face sheets 50-μm thick. The use of microfiche masks for photolithography enables fabrication of finer features.[11] Cell diameters and wall widths approximately 150 and 15 μm, respectively, can be obtained with this technique. Such length scales might allow realization of small components.

II. MICROGRIDS AND SANDWICH BEAMS

A. Metallic cores

Figure 2(a) shows the procedure used to fabricate the metallic microgrids.[10] Silicon (Si) wafers were coated with a 10-nm-thick layer of chromium (Cr) and then a 100-nm-thick layer of gold (Au) by electron-beam evaporation. The Si wafers were subsequently coated with a 500-μm thick layer of SU-8 photoresist (Micro-Chem Corporation, Newton, MA). Following a rapid prototyping methodology, the photoresist was patterned with the negative images of the desired grid using transparency film as the mask in photolithography.[12] The grid patterns were created with a computer-aided program and printed at high resolution (3386 dots/in., dpi) on these transparency sheets (the masks). Microfiche masks[11] have higher resolution than the polymeric transparency sheets and were used to produce those grid configurations with unit cell dimensions smaller than 300 μm or cell walls thinner than 30 μm. Nickel (Ni) was deposited on Si wafers using a commercial nickel sulfamate bath (Nickel "S", Technic Inc., Cranston, RI) at 40 °C at a current density of 10 mA/cm^2 for four days. After electrodeposition, the Ni grids, while still attached to the photoresist, were separated from the Si wafers by heating at 300 °C. Finally, the photoresist was dissolved in concentrated sulfuric acid to yield freestanding nickel grids.

To prepare sandwich beams, two sheets of Ni with a thickness of 50 μm (Goodfellow Corporation, Berwyn, PA) were covered with adhesive tape (Scotch Magic Tape, 3M, Minneapolis, MN) on one side and electroplated on the uncovered side with a 5-μm-thick layer of

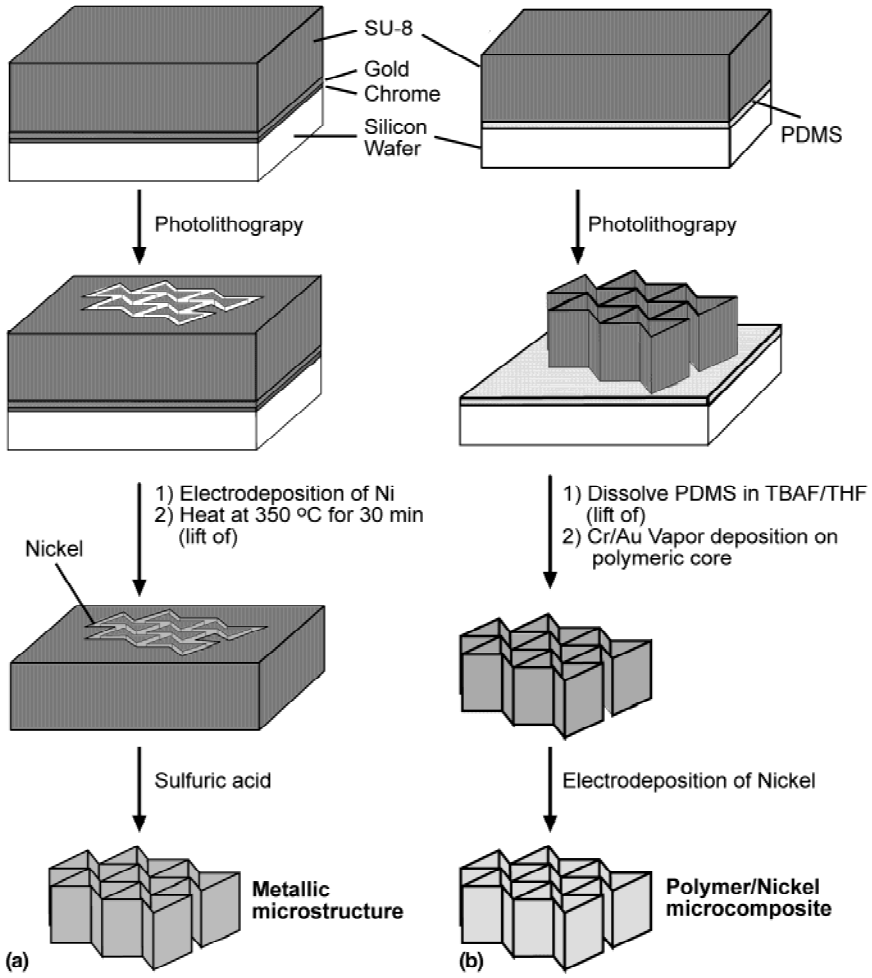

FIG. 2. Schematic depiction of the fabrication methods for (a) the metallic grids and (b) the polymer (SU-8)/nickel composite grids.

80 Pb/20 Sn solder using a commercial solution (Learonal Inc., Freeport, NY). The adhesive tape was then removed, the metallic sheets were rinsed with deionized water, and the grids were sandwiched between two face sheets and heated, in a nitrogen ambient, to 350 °C to allow the solder to flow [see Fig. 3(a)]. Scanning electron microscope images (Fig. 4) reveal that the solder partially fills the open space of the core grid.

B. Polymer/metal microcomposite cores

Figure 2(b) summarizes the fabrication of the SU-8/nickel microcomposite cores. First, a 50-μm-thick layer of polydimethylsiloxane (PDMS) was spin coated on Si wafers. The PDMS films were then cured at 70 °C for 2 h. The surface of the PDMS was oxidized in a plasma cleaner (Harrick PDC-32G, Harrick Scientific Corp., Ossining, NY) for 2 min, and the wafers were coated with a 500-μm-thick layer of SU-8 photoresist. The positive images of the desired grid patterns were reproduced with the SU-8 photoresist using the rapid prototyping methodology described above (Sec. IIA).[12] The resulting polymer grids—consisting of cured photoresist—were subsequently separated from the Si substrate by dissolving the PDMS in a 1 M solution of tetrabutylammonium fluoride (TBAF) in tetrahydrofuran (THF). Further details of the use of PDMS as a sacrificial layer are available elsewhere.[13] The free-standing SU-8 grids were coated with a 10-nm layer of Cr and then a 100-nm layer of Au by shadow evaporation at a tilt angle of approximately 30 ° with respect to the metal source to ensure maximum exposure of the SU-8 surfaces to the metallic evaporant. Finally, a 25-μm-thick layer of Ni was electrodeposited on the grids using the method described above (Sec. IIA). The polymer/metal grids were bonded to the 50-μm-thick Ni face sheets using a metallic composite adhesive (Durabond 950, Cotronics Corporation, Brooklyn, NY) and cured at 120 °C for 2 h [see Fig. 3(b)]. In general, the thickness of the adhesive layer varied between 5 and 15 μm.

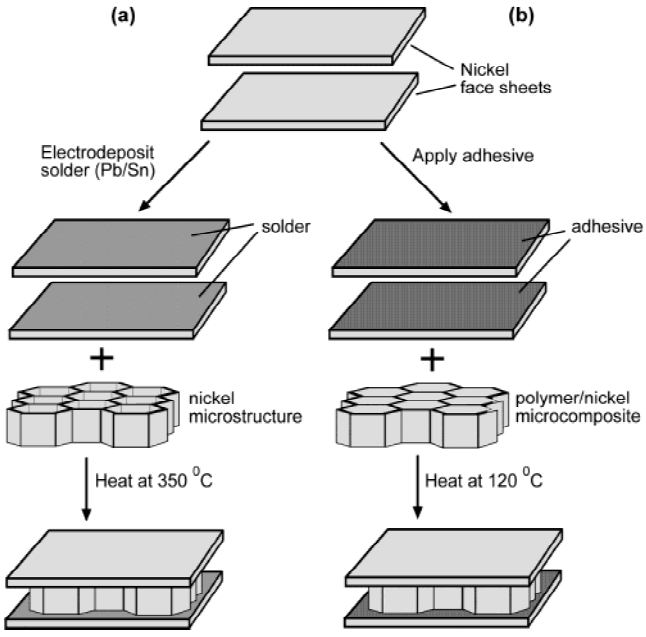

FIG. 3. Schematic depiction of the methods used to bond the metallic face sheets (a) to the metallic core using solder and (b) to the polymer/metal composite core using adhesive.

C. Microgrids and sandwich construction

Scanning electron microscope images of typical examples of metallic grids and of polymer/nickel composite grids are shown in Figs. 5(a) and 5(b), respectively. Images of the SU-8/Ni microcomposite cores [Fig. 5(b)] affirm good coverage of the polymer core by the electrodeposited Ni. Figure 5(c) shows examples of sandwich structures: one with a metallic grid and one with a composite grid. The relative density of each material was determined from scanning electron microscope images by measuring the area fraction. It is designated ρ^*/ρ_s (where ρ^* is the density of the core material and ρ_s the density of the solid) and varied between 0.2 and 0.3.

III. STRUCTURAL PERFORMANCE

A. Measurements

Four-point bending tests were employed to assess the bending stiffness, failure mode, and strength. A schematic of the experimental setup, including the definitions of the different parameters used, is shown in Fig. 6. The tests used an outer load span $L = 31.75$ mm and a distance between the outer and the inner load lines $a = 7.94$ mm ($a/L = 0.25$), and the typical specimen width, b, was 10 mm. The face sheet thickness was fixed at $t = 50$ μm, while the core thickness, c, was allowed to vary between 100 μm and 1 mm. All tests were performed

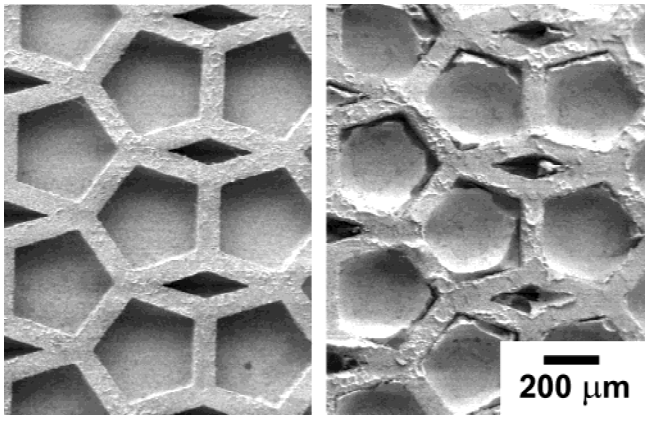

FIG. 4. SEM micrographs showing a core structure—periodic Durer's pentiling—without (left) and with (right) the excess solder in the core (only one face sheet attached).

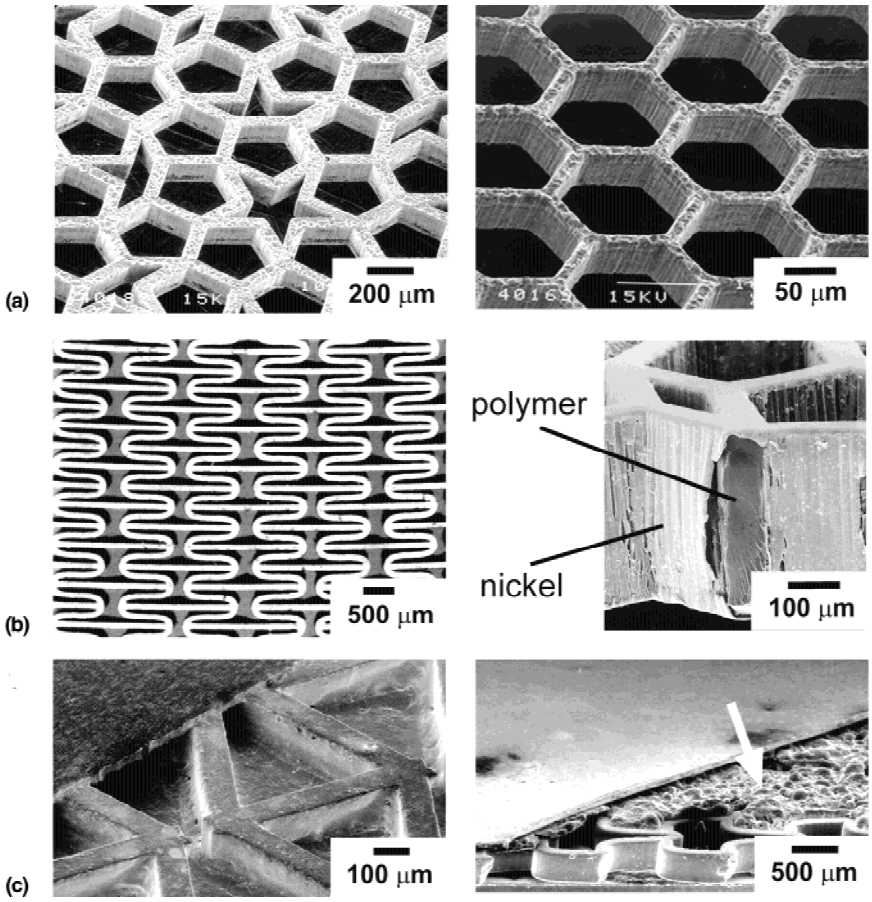

FIG. 5. SEM micrographs of some microgrids and some sandwich beam structures: (a) two examples of metallic grid structures, the one to the left fabricated using a transparency film as the mask in photolithography and the one to the right fabricated using microfiche film as the mask; (b) polymer/nickel composite grid and a fracture profile clearly showing the polymeric core and metallic shell of the grid; (c) sandwich beam structures with a metallic core (left) and with a composite core (right). The arrow indicates residual adhesive.

using a hydraulically actuated mechanical testing machine operating in displacement control at a displacement rate of 20 μm/s. The load point displacements were measured using a linear variable displacement transducer (LVDT), and the applied load was monitored with a 50 N load cell. The core orientation with respect to the loading axis is indicated on Fig. 1. Most cores were tested in the "stiff" orientation. The two exceptions were the nickel/SU-8 beams with the NPR core [Fig. 1(c)] and the beams with the Penrose core [Fig. 1(i)]. In both cases, a "soft" orientation was aligned with the load axis.

A load–displacement response representative of most beams tested in the "stiff" orientation is shown in Fig. 7(a). The load increases linearly with the displacement until yielding initiates, beyond which the deformation is nonlinear and irrecoverable. Subsequent to yielding there is some hardening followed by attainment of a limit load. The nonlinearity of most beams is determined by face sheet yielding, as evident from the remnant curvature after unloading. The beams tested in the "soft" orientation behave differently. Such beams exhibit plastic displacements at essentially constant load [Fig. 7(b)]. The trends in flexural rigidity and limit load with core height for all cores are presented on Figs. 8(a) and 8(b), respectively.

B. Stiffness and strength

For the well-bonded "stiff" cores, the in-plane shear stiffness is sufficiently large that the overall displacement is dominated by the bending of the face sheets about the centroid of the sandwich beam such that [Appendix, Eq. (A6)]

$$\delta \approx \frac{PL^3}{B_1(EI)_{\mathrm{eq}}} \quad . \tag{1}$$

Accordingly, $(El)_{\mathrm{eq}}$ has been calculated from the load–displacement curves, using Eq. (1). It is plotted on Fig. 8(a), as a function of c/t, where it is compared with the beam theory prediction [Appendix, Eq. (A2b)]. The correspondence between the measurements and the beam-theory prediction affirms that the contribution to

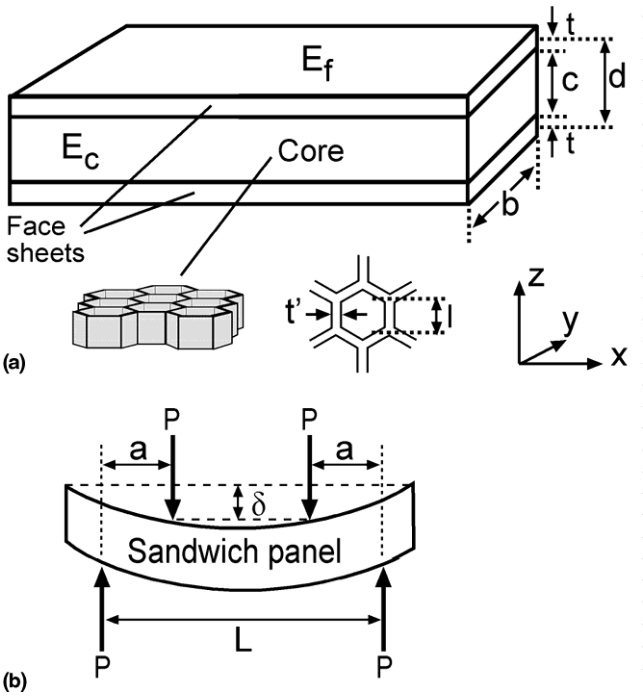

FIG. 6. Schematic of the four-point bending test, specimen geometry, and orientation.

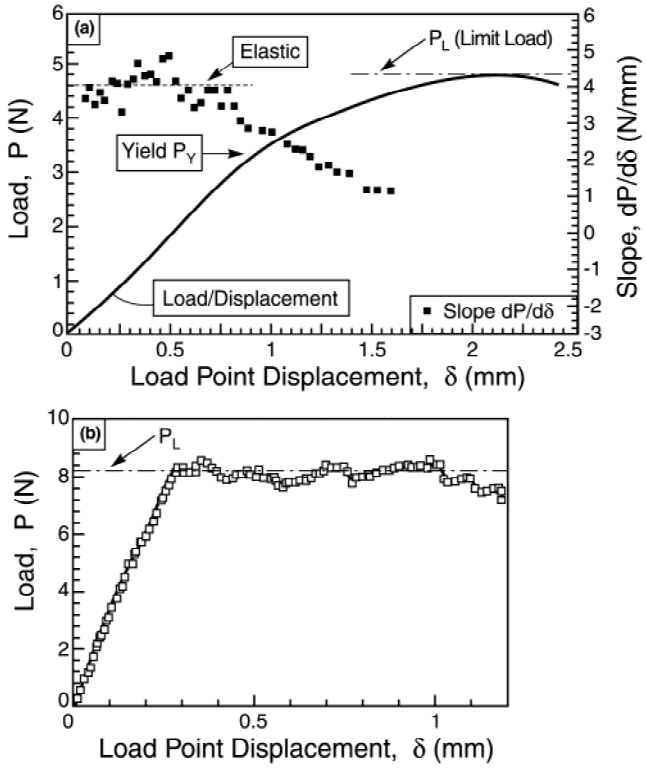

FIG. 7. Representative load–displacement curves for (a) the Ni-core sandwich beam fabricated with the quasiperiodic Kepler's pentiling structure depicted in Fig. 1(g) and (b) the polymer/metal composite-core sandwich beam fabricated with the NPR structure depicted in Fig. 1(c).

the compliance from these cores is negligible. The exceptions are the two cases denoted "debonding", wherein insufficient interface adhesion diminished the stiffness below the expected levels. The two cores tested in the "soft" orientation [Figs. 1(c) and 1(i)] exhibit stiffness lower than Eq. (A2b) by about a factor about 4. The high compliance arises because the out-of-plane shear response of these cores is small. Estimates of the associated out-of-plane shear modulus, G^*, have been obtained from the load point displacements, using Eq. (A1a). These indicate that for both cores, $G^* = 0.1$ GPa, almost 2 orders of magnitude smaller than the shear modulus for the hexagonal honeycomb at the same relative density, $G^* \sim 8$ GPa [Appendix, Eq. (A3)].

For the specimens with metallic cores, upon using a yield strength for the nickel face sheet estimated from microindentation (270 MPa), the yield loads [Fig. 8(b)] are found to be in reasonable agreement with the beam theory result [Appendix, Eq. (A7)]. The variability in the measured loads is attributed to uneven overall specimen thickness arising from nonuniformity in the solder thickness. In some cases, excess solder contributed to the load capacity. Conversely, the loads sustained by some specimens with polymer–metal composite cores are appreciably lower than the beam theory prediction. The disparity is caused either by debonding and/or brittle fracture of the core. The low values measured for the "soft" cores arise because the limit loads are governed by core shear (Appendix) rather than face yielding. The shear yield strength of these cores is ascertained from Eq. (A8) as, $\tau_y^c \sim 5$ MPa, almost 1 order of magnitude lower than that for a honeycomb core at the same relative density.

C. Minimum weight designs

Minimum weight designs for beams with metallic hexagonal honeycomb cores[14] that fail simultaneously by face sheet yielding and by core buckling would be quite different from the cores investigated in this study. They would have core thickness $c = 3.25$ mm, face thickness $t = 8.13$ μm, and core density $\rho^*/\rho_s = 0.0075$ (other dimensions being comparable). The cell wall thickness of a honeycomb with an optimized core density would be about 1 μm for the cell sizes investigated in this study. The corresponding stiffness would be approximately 0.12 MN/m, and the limit load would be approximately 5 N, that is over 1 order of magnitude stiffer than the beams fabricated for this study but comparable in failure load. Such superior performance could be achieved by increasing the core height relative to the face sheet thickness and, correspondingly, by reducing the core density. Recent studies[13,16] have demonstrated the capability of producing high-aspect ratio core materials. Fabrication of low density core structures with relative densities of less

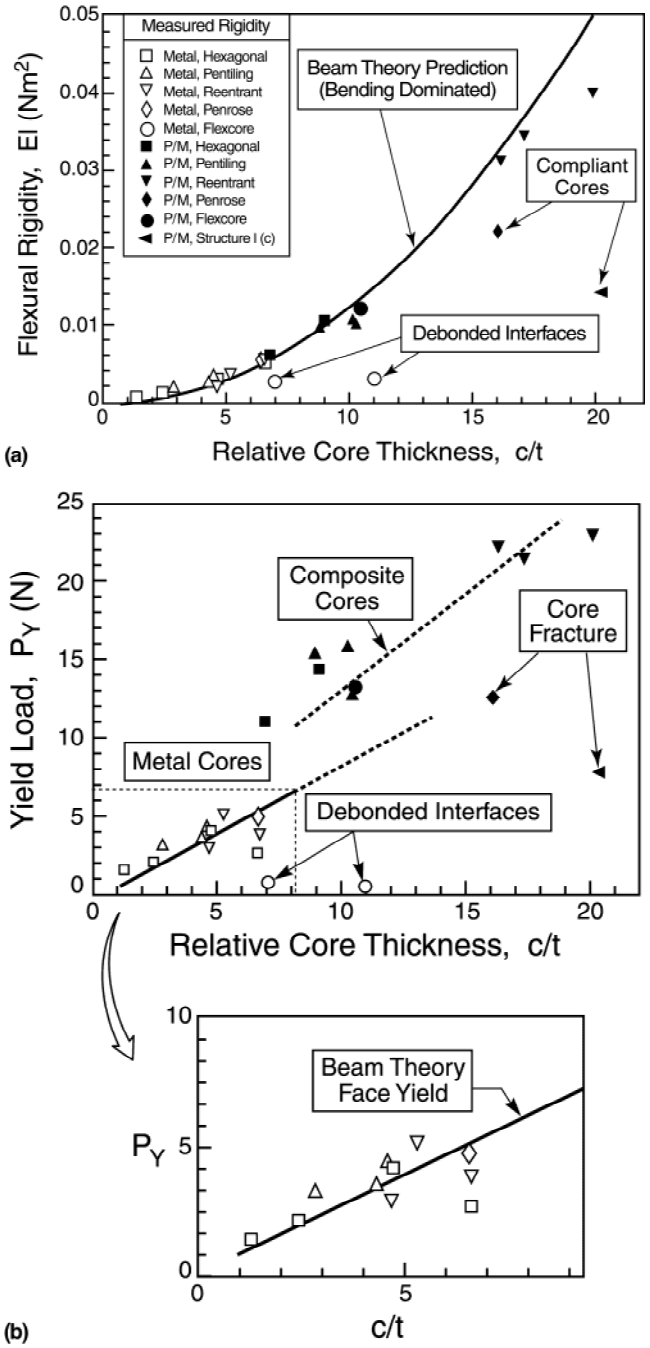

FIG. 8. Variation of (a) flexural rigidity $(EI)_{eq}$ and (b) failure load as a function of the core height normalized by the face sheet thickness (c/t). The solid line represents the theoretical prediction while the open and the closed symbols represent the experimental data obtained from the sandwich beams made with the Ni and polymer/Ni composite cores, respectively.

than 1%, however, is not practical with the technology described in this paper unless the cell diameter is increased to about 5 mm. Furthermore, it should be noted that modifying the cell size can potentially instigate a change in the failure modes and the optimum core density will have to be reanalyzed. Further advances in fabrication methods will enable realization of efficient micro- and mesoscale sandwich components for future application.

III. CONCLUSION

A convenient fabrication of metallic and polymer/metal composite *microscale* sandwich panels with cell diameters and wall widths down to 150 and 15 μm, respectively, has been demonstrated. The rapid prototyping strategy presented here uses readily available techniques—photolithography, electrodeposition, and face-sheet bonding—for the fabrication of microscale sandwich beams; in the past, such structures have been accessible primarily by the synchrotron-based LIGA process.

The bending responses of the sandwich beams presented in this paper are found to be insensitive to the core configuration except in two cases. The dimensions of the cores are far from optimum. Recent investigations[14,15] provide guidelines for more efficient—i.e., higher strength-to-weight ratio—structural design. A significant reduction in the core density is a prerequisite. Moreover, the ability to make high-aspect ratio cores is also a necessary step. We demonstrated recently the capability of fabricating high-aspect ratio cores using PDMS as a sacrificial material.[13,16] Further advances in microscale materials processing technology will enable fabrication of efficient micro- and mesoscale sandwich components for future applications in microstructures in which either low weight or inertial mass is relevant, together with tuned mechanical properties. Possible examples include small air vehicles, hard disk drive arms, and agile millimeter-wavelength antennae.

REFERENCES

1. H. Allen, *Analysis and Design of Structural Sandwich Panels* (Pergamon Press, Oxford, United Kingdom, 1969).
2. *Honeycomb and Prepreg in Sandwich Construction* (Hexcel Corporation, Dublin, CA, 1974).
3. L.J. Gibson and M.F. Ashby, *Cellular Solids—Structure and Properties*, 2nd ed. (Cambridge University Press, Cambridge, United Kingdom, 1997).
4. S.T. Brittain, Y. Sugimura, O.J.A. Schueller, A.G. Evans, and G.M. Whitesides, J. Microelectromech. Syst. (in press).
5. P.F. Jacobs, *Rapid Prototyping and Manufacturing: Fundamentals of Stereolithography* (Society of Manufacturing Engineers, Dearborn, MI, 1992).
6. A. Alderson, J. Rasburn, S. Ameer-Beg, P.G. Mullarkey, W. Perrie, and K.E. Evans, Ind. Eng. Chem. Res. **39,** 654 (2000).
7. M. Madou, *Fundamentals of Microfabrication* (CRC Press, New York, 1997).
8. Y. Xia, and G.M. Whitesides, Angew. Chem., Int. Ed. Engl. **37,** 550 (1998).
9. B. Xu, F. Arias, S.T. Brittain, X.-M. Zhao, B. Grzybowski, S. Torquato, and G.M. Whitesides, Adv. Mater. **11,** 1186 (1999).
10. B. Xu, F. Arias, and G.M. Whitesides, Adv. Mater. **11,** 492 (1999).

11. T. Deng, J. Tien, B. Xu, and G.M. Whitesides, Langmuir **15,** 6575 (1999); T. Deng, H. Wu, S.T. Brittain, and G.M. Whitesides, Anal. Chem. **72,** 3176 (2000).
12. D. Qin, Y. Xia, and G.M. Whitesides, Adv. Mater. **8,** 917 (1996).
13. F. Arias, S.R.J. Oliver, B. Xu, R.E. Holmlin, and G.M. Whitesides (submitted for publication).
14. N. Wicks and J.W. Hutchinson, Int. J. Solids Struct. (in press).
15. H. Bart-Smith, J.W. Hutchinson, and A.G. Evans, Int. J. Mech. Sci. (in press).
16. Y. Sugimura, Design and Characterization of Small-Scale Sandwich Beams Fabricated by Photolithography and Electrodeposition, presented at The 2000 International Mechanical Engineering Congress and Exposition, Orlando, FL, Nov 8, 2000.

APPENDIX

A. Bending stiffness of sandwich beams

The load point displacement of a sandwich beam under bending consists of two terms, that due to moment, δ_b, and that due to core shear, δ_s,[1,3]

$$\delta = \delta_b + \delta_s = \frac{PL^3}{B_1(EI)_{eq}} + \frac{PL}{B_2(AG)_{eq}} \quad , \qquad \text{(A1a)}$$

where B_1 and B_2 are constants that depend on the loading configuration. For four point bending, $B_1 = 48$ and $B_2 = 4$.[4] The quantities $(EI)_{eq}$ and $(AG)_{eq}$ refer to the equivalent flexural and shear rigidities, respectively. The parameters P and δ are the applied load and load point displacement (Fig. 6). Note that the ratio of the contributions from bending and shear is given by

$$\delta_b/\delta_s = \frac{B_2(AG)_{eq}L^2}{B_1(EI)_{eq}} \quad . \qquad \text{(A1b)}$$

Using the parallel axis theorem for a beam with a rectangular cross-section, the equivalent flexural rigidity is[1,3]

$$(EI)_{eq} = E_f\frac{bt^3}{6} + E_c\frac{bc^3}{12} + E_f\frac{btd^2}{2} \quad , \qquad \text{(A2a)}$$

where E_f and E_c are the in-plane Young's modulus for the face sheet and the core material and $d = c + t$. The first two terms describe the bending stiffness of the face sheets and the core about their own centroids. When the beams are optimized for minimum weight, t/d and E_c/E_f are small[3] and, consequently, the first two terms in Eq. (A2a) are small relative to the third. In addition, at small t/d, then $d \approx c$. Accordingly, the flexural rigidity reduces to[1,3]

$$(EI)_{eq} = E_f\frac{btc^2}{2} \quad . \qquad \text{(A2b)}$$

The corresponding shear rigidity is given by[1,3]

$$(AG)_{eq} = bcG^* \quad , \qquad \text{(A3)}$$

where G^* is the shear modulus of the core material. Further insight about the bending response can be obtained for hexagonal honeycomb cores, which have been comprehensively analyzed.[14] Their shear modulus varies linearly with the relative core density:[3]

$$G^*/E_s \approx 0.2\,\rho^*/\rho_s \qquad \text{(A4)}$$

where E_s is the Young's modulus for the core material. Inserting Eqs. (A2b)–(A4) into Eq. (A1b), the displacement ratio for hexagonal honeycombs becomes ($E_s = E_f$):

$$\delta_b/\delta_s = \frac{0.4B_2L^2\,\rho^*/\rho_s}{B_1tc} \quad . \qquad \text{(A5)}$$

At the relatively large densities used in this study ($\rho^*/\rho_s > 0.2$), this ratio is large and the overall displacement is dominated by the bending of the face sheets, reducing Eq. (A1a) to

$$\delta \approx \frac{PL^3}{B_1(EI)_{eq}} \quad . \qquad \text{(A6)}$$

This is the result used in the text. For other core configurations as well as for hexagonal honeycombs having lower relative density, shearing of the core causes the beam to be more compliant. This issue will also be addressed in the text.

B. Limit loads

In sandwich beams, various mechanisms limit the load capacity in bending. The mechanisms involve face yielding, core shear, wrinkling of the faces, and buckling of the core. The associated loads, derived from beam theory, are summarized here. The derivations are elaborated elsewhere.[14,15] The result presented for face yield applies to all cores, while the face wrinkling, core yielding, and core buckling results are specialized for hexagonal honeycombs.

(1) *Face sheet yielding* occurs when the normal stress reaches the yield strength, σ_y^f. Beam theory indicates that the load at the onset of face sheet yielding can be expressed as[14,15]

$$P = B_3bc\left(\frac{t}{L}\right)\sigma_y^f \quad . \qquad \text{(A7)}$$

(2) *Face wrinkling* occurs in beams with hexagonal cores when the face sheet, constrained by the underlying hexagonal cell, satisfies the local buckling condition (A

tactic assumption was made that the cell wall thickness is small compared to the cell wall length upon deriving this expression.):[14]

$$P = B_4 bc\left(\frac{t^3}{Ll^2}\right)\frac{E_f}{(1-\upsilon_f^2)} \quad . \tag{A8}$$

(3) *Core yielding* happens when the average shear stress in the hexagonal cell wall reaches its shear yield strength, τ_Y^c, such that[14]

$$P = B_5 bc\left(\frac{\tau_y^c}{l}\right)\tau_y^c \quad . \tag{A9}$$

For a hexagonal honeycomb core, τ_Y^c is related to the tensile yield strength, σ_y^c, of the material by[14]

$$\tau_y^c = \sigma_y^c\sqrt{3} \quad . \tag{A10}$$

(4) *Buckling* of the cell wall in a hexagonal honeycomb core, when regarded as simply supported, occurs at a load:[14]

$$P = B_6 bc\left(\frac{t'}{l}\right)\left[5.35\left(\frac{t'}{l}\right)^2 + 4\left(\frac{t'}{c}\right)^2\right]\frac{E_s}{1-\upsilon_s^2} \quad \text{for } l > c \quad , \tag{A10a}$$

$$P = B_6 bc\left(\frac{t'}{l}\right)\left[4\left(\frac{t'}{l}\right)^2 + 5.35\left(\frac{t'}{c}\right)^2\right]\frac{E_s}{1-\upsilon_s^2} \quad \text{for } l < c \quad . \tag{A10b}$$

In the above, B_i are constants wherein for four-point bending with $a/L = 0.25$, $B_1 = 48$, $B_2 = 4$, $B_3 = 4$, $B_4 = 0.72$, $B_5 = 0.33$, and $B_6 = 0.47$.[4,14]

ACKNOWLEDGMENTS

This work was supported in part by DARPA [Microelectromechanic System (MEMS) program], NSF Grant ECS-9729405, and by ARO-MURI Grant DAAH04-95-1-0102. MRSEC-shared facilities supported by the NSF under Grant DMR-9809363 were used. P.J.A.K. acknowledges the Netherlands Organization for Scientific Research (NWO) for a postdoctoral fellowship. F.A. and B.X. thank the NIH for postdoctoral support.